Strong suppression of graphene growth by sulfur superstructure on a nickel substrate

Keisuke Sagisaka [1,*] Jun Nara,[2] Jill K. Wenderott,[3,†] Ryo Kadowaki,[4] Akane Maruta,[4]
Tadashi Abukawa [4] and Daisuke Fujita[1]

[1]*Research Center for Advanced Measurement and Characterization, National Institute for Materials Science 1-2-1 Sengen, Tsukuba, Ibaraki 305-0047, Japan*

[2]*International Center for Materials Nanoarchitectonics (MANA), National Institute for Materials Science 1-1 Namiki, Tsukuba, Ibaraki 305-0044, Japan*

[3]*Department of Materials Science and Engineering, University of Michigan Ann Arbor, Michigan 48109, USA*

[4]*Institute of Multidisciplinary Research for Advanced Materials, Tohoku University, Sendai 980-8577, Japan*

The formation of multilayer graphene on a nickel substrate is usually unavoidable due to the precipitation of carbon upon cooling after the growth of the single layer of graphene. We found that the growth rate of graphene on a Ni(110) surface was markedly reduced when the surface was covered by sulfur atoms arranged in a $c(2 \times 2)$ periodicity. An atomistic survey by scanning tunneling microscopy revealed a compression of the sulfur superstructure as a result of the growth of graphene-covered regions. Photoelectron emission microscopy showed that the growth rate of graphene is linear with time, which indicates that carbon atoms are supplied only at the growth front of graphene islands. Density functional theory calculations rationalized these experimental results and suggested a mechanism for suppressing the growth of graphene. Sulfur atoms might extend the utility of nickel substrates for the production of single-layer graphene or nanographenes.

I. INTRODUCTION

Studies on graphene generally focus on single layer graphene (SLG), bilayer graphene (BLG), or nanographene (NG), including graphene nanoribbons, as many of the excellent electronic, optical, mechanical, and magnetic properties result from the presence of these forms [1–11]. The production of these desirable forms of graphene requires fine control of the number and shape of layers, as well as the crystalline quality. Chemical vapor deposition (CVD) is the technique most widely used to produce large-area, high-quality samples of graphene [12]. This technique has been demonstrated using various metal surfaces, such as Cu, Ni, Pt, Ru, Rh, Ir, Fe, Au, and their alloys [13]. Among these metals, copper and nickel are especially relevant as a substrate, owing to low cost and high availability. The synthesis of graphene is believed to follow one of two reaction pathways: (i) direct formation of graphene from carbon produced by the decomposition of hydrocarbons on a catalyst surface or (ii) decomposition of the hydrocarbon at the surface and diffusion into the catalyst, followed by segregation of dissolved carbon from the subsurface of a catalyst substrate [14,15]. Which of these reactions predominates depends on the solubility of carbon in the substrate metal; pathways (i) and (ii) typically occur on copper and nickel substrates, respectively [14]. In the case of nickel as a substrate, the synthesis of graphene through segregation is quite rapid because of the high concentration of

carbon present, owing to its large solubility in the substrate. However, this unique property becomes a drawback if it is necessary to control the number of layers. SLG forms at about the segregation temperature (T_S) [16,17] but this process must be followed by cooling of the substrate, which usually causes precipitation and subsequent stratification of graphene at temperatures below T_S [16,17]. As a consequence, CVD [18,19] and direct-segregation methods [20,21] using a nickel substrate generally produce multilayer graphene or graphene with a nonhomogeneous thickness [22]. To avoid this multilayer growth, SLG production on nickel surfaces has been engineered by controlling the conditions for CVD [23,24], by using a binary metal alloy [25] or nickel carbide [26], by using a thin film of nickel on graphite [27], or by using aluminum barriers to limit the diffusion of carbon [28].

We previously reported the growth of graphene islands in coexistence with sulfur on a Ni(110) surface, but the effect of the sulfur atoms on the growth of the graphene remained unclear [29]. We also noted that the growth speed of graphene was extremely slow, which was likely related to the presence of sulfur on the surface. In this paper, we experimentally and theoretically address the impact of sulfur atoms on the growth of graphene on the Ni(110) surface. Impurity sulfur atoms segregate to form a superstructure of the $c(2 \times 2)$ periodicity at high temperature ($\sim$1000 °C), at which the formation of graphene does not take place. Upon cooling the sample, the growth of graphene is initiated but its speed is largely suppressed by the presence of the sulfur superstructure, as the advancement of graphene edges and the supply of carbon to the edges are restricted by the sulfur atoms. The fundamental mechanism behind these phenomena is the strong repulsion between carbon and sulfur atoms both at the surface and

----
*SAGISAKA.Keisuke@nims.go.jp
†Current address: Department of Materials Science and Engineering, Northwestern University Evanston, IL 60201, USA.

subsurface of nickel. This intriguing repulsive effect that we have demonstrated experimentally and theoretically imparts a controllable graphene growth speed and leads the way to the production of SLG or NG on a nickel substrate.

II. METHODS

A. Preparation of the carbon-doped Ni(110) substrate and the growth of graphene

Single-crystal nickel substrates with a (110) surface were placed in a carbon crucible together with high-purity carbon powder. The crucible was heated in a furnace at 800 °C under a vacuum of $\sim 10^{-4}$ Pa for three weeks to dope the nickel crystals with carbon. The concentration of carbon in the doped nickel was estimated by a chemical analysis to be 0.44 atom % or 4.0×10^{20} cm^{-3}. This number is close to the reported solubility of carbon atoms in nickel at 800 °C (0.49 atom %) [30,31]. After the doping, the crystal was polished to a mirror surface with alumina powder, then subjected to ultrasonic cleaning in acetone.

To grow graphene, we exploited the segregation of carbon in ultrahigh vacuum (UHV) environments. After loading into the UHV chamber, the crystal was initially heated to 1000 °C for one minute to remove any oxide layer or surface impurities. At this temperature, most carbon on the surface should dissolve in the substrate while impurity sulfur will segregate to the surface to create a c(2 × 2)-S superstructure. Afterward, graphene growth was performed by carbon segregation upon cooling to room temperature. Growth of the graphene was controlled by varying the cooling rate between 750 and 850 °C. The temperature of the sample was monitored with an infrared pyromter ($\epsilon = 0.1$).

B. Characterization methods

Scanning tunneling microscopy (STM) and low-energy electron-diffraction (LEED) measurements were performed in a low-temperature STM system (Unisoku USM-1300). After graphene had been grown in the preparation chamber (base pressure $<5.0 \times 10^{-9}$ Pa) of a LEED apparatus (OCI 800), the sample was loaded into the scanning tunneling microscope, and STM was performed at 78 K by using a polycrystalline tungsten tip. After the STM and LEED measurements, the sample was exposed to air and transferred to a helium-ion microscope (Zeiss Orion-Plus) [32,33]. HIM images were recorded with a beam current of 2.2 pA and an acceleration voltage of 25 kV. Real-time observations of graphene growth were conducted on a photoelectron emission microscopy (PEEM) system equipped with a Hg lamp (~ 4.9 eV) as a UV source (Omicron IS-PEEM with a microanalyzer).

C. Computational methods

Computations were conducted by using PHASE/0 code [34], which is based on DFT [35] and the projector augmented pseudopotential scheme [36] with plane wave basis sets [37]. For the exchange correlation term, the Perdew-Burke-Ernzerhof form was used [38]. For the van der Waals interactions, the DFT-D2 method was applied [39]. For the activation-barrier search, we employed the nudged
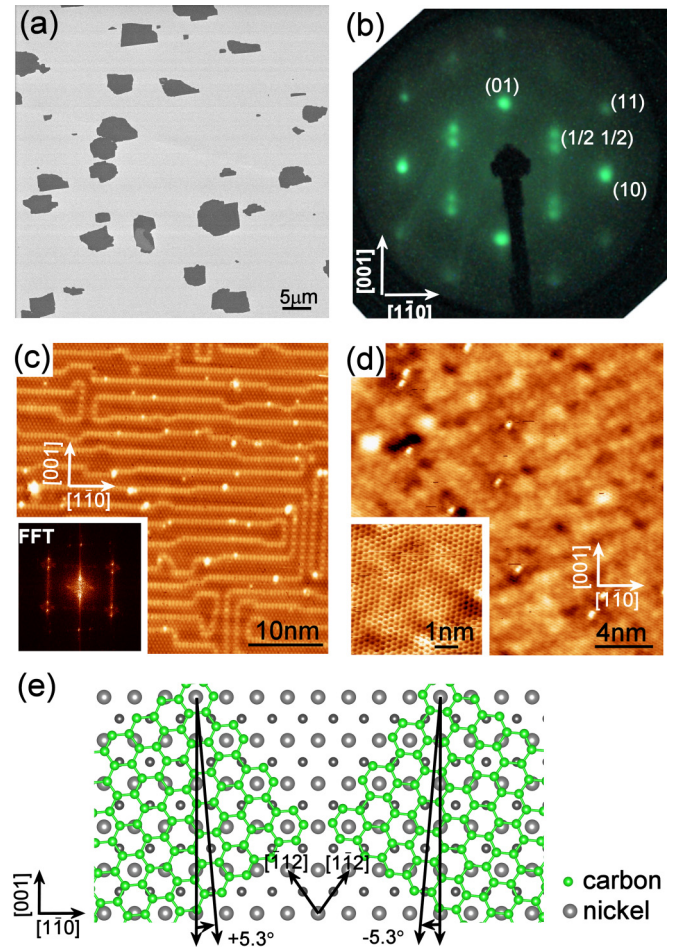

FIG. 1. Graphene islands grown on a C-doped Ni(110) substrate through segregation. (a) Helium-ion microscopy image of the sample after cooling at 3.3 °C/s from 1000 °C to 600 °C, followed by further cooling to room temperature. He$^+$ acceleration voltage = 25 kV. (b) LEED pattern from the same sample surface. Incident electron energy = 80.5 eV. (c) STM image from the region outside the SLG islands [light grey region in (a)]. The inset shows the corresponding FFT image. $V_s = +1.0$ V, $I = 0.1$ nA, $T = 78$ K. (d) STM image from an SLG island [dark gray patch in (a)]. The inset shows an atomic-resolution image. $V_s = +0.5$ V, $I = 0.2$ nA, $T = 78$ K. (e) Stick-and-ball model showing the two types of orientation for SLG stacked on a Ni(110) surface identified by a RHEED analysis.

elastic band method in combination with the force-inversion method [40,41]. The cutoff energy for the plane wave basis was 25 Ry. The number of k points sampled in the Brillouin zone was more than 16 × 16 per 1 × 1 surface unit cell. Slab calculations were carried out with twelve Ni layers for Fig. 4, six Ni layers for Fig. S6 in the Supplemental Material [42], and four Ni layers for Fig. S7-S10 in the Supplemental Material [42]. All calculations were performed with a vacuum region corresponding to six nickel layers.

III. RESULTS AND DISCUSSION

A. Characterization of graphene grown on the Ni(110) surface

Figure 1(a) shows helium-ion microscopy (HIM) images of the (110) surface of a carbon-doped single crystal of nickel

TABLE I. Conditions for growth of graphene on Ni surfaces.

	This paper	Yu *et al.* [20]	Kim *et al.* [18]	Reina *et al.* [19]	Baraton *et al.* [21]
Method	segregation	segregation	CVD	CVD	segregation
Cooling rate ($°Cs^{-1}$)	3	10	0.5–10	(5–10 min)[a]	(30 min) [a]
Growth temp (°C)	$\leqslant 1000$	$\leqslant 1000$	$\leqslant 1000$	900-1000	900
Thickness	island	multi (1-4L)	multi (1-5L)	multi (1-10L)	multi

[a]This work showed growth time instead of cooling rate.

after heating to 1000 °C for 1 minute, followed by cooling at 3 °C/s to 600 °C and subsequent cooling to room temperature. The dark gray patches generally correspond to SLG islands grown through surface segregation of carbon atoms. One patch, however, contained a bilayer region. The graphene islands were typically several micrometers in size and covered approximately 12% of the surface of the substrate. This result is remarkable because, although the substrate contained a high concentration of carbon and the heating temperature and cooling rate were similar to those in recipes used in previous reports on the synthesis of multilayer graphene [18–21], the rate of growth of graphene in the current study was extremely slow and the graphene formed single layer islands almost exclusively, rather than multilayer graphene (Table I).

A LEED study on the same surface showed spots from the substrate lattice [(1,0), (0,1), and (1,1)] and additional double spots around (1/2, 1/2) [Fig. 1(b)]. The coverage of graphene was so low that diffraction spots from the graphene islands were not visible by LEED. The origin of the (1/2, 1/2) spots was attributed to a superstructure produced by impurity sulfur atoms segregated from the substrate, as detected by AES (see Fig. S1) and by atom-resolved STM observations (Fig. 2). A separate chemical analysis estimated that a nickel plate with the same purity (99.999%) to that of the single crystal of Ni used in the graphene-growth experiments contained as much as 0.0037 at% sulfur. It has been known for some time that segregation of sulfur reduces the surface energy of a nickel surface and gives rise to a c(2 × 2)-S superstructure on Ni(110) [Fig. 2(c)], in which each sulfur atom is located in a twofold hollow site and the coverage (Θ) corresponds to 0.5 monolayers [43–46]. Such sulfur superstructures were found in the regions outside the graphene islands [Fig. 1(c)]. The STM image of this region was dominated by round protrusions separated by 0.709 and 0.507 nm along the [001] and [1$\bar{1}$0] crystal orientations, respectively, nearly equal to a 2 × 2 periodicity with respect to the substrate lattice. A more striking feature in Fig. 1(c) is that a number of corrugated lines are discernible along both the [001] and [1$\bar{1}$0] crystal orientations in the c(2 × 2)-S phase. Each of these lines actually consists of rows, each two sulfur atoms in width, which are the origin of the double diffraction spots at (1/2, 1/2) in the LEED image in Fig. 1(b). A fast-Fourier transform (FFT) of the atomically resolved STM image in Fig. 1(c) duplicated the double-spot image [see the inset in Fig. 1(c)], in a similar manner to the LEED pattern. From these observations, we hypothesize that the extremely slow growth rate of the graphene is caused by the presence of sulfur on the substrate surface. Underscoring this point, we confirmed that multilayer graphene grew on the same carbon-doped substrate after the sulfur atoms had been

removed from the surface by argon-ion sputtering (Fig. S2 in the Supplemental Material [42]).

A typical STM image of the interior of an SLG island is shown in Fig. 1(d). The crystallinity of the SLG was excellent in the internal regions tens to hundreds of nanometers from the edges of the island. The root-mean-square roughness in the image area was 6.4 pm and the defect density was $0.038\ nm^{-2}$. Reflection high-energy electron-diffraction (RHEED) measurements (Fig. S3) confirmed that the SLG islands adopt two types of orientation in which the armchair axis of the graphene is aligned to the [1$\bar{1}$2] or [$\bar{1}$12] orientation of the substrate, respectively, as depicted in Fig. 1(e). Previous studies on graphene growth on the (110) surfaces of Cu [47] and Ni [48,49] reported the formation of moiré patterns, indicating a
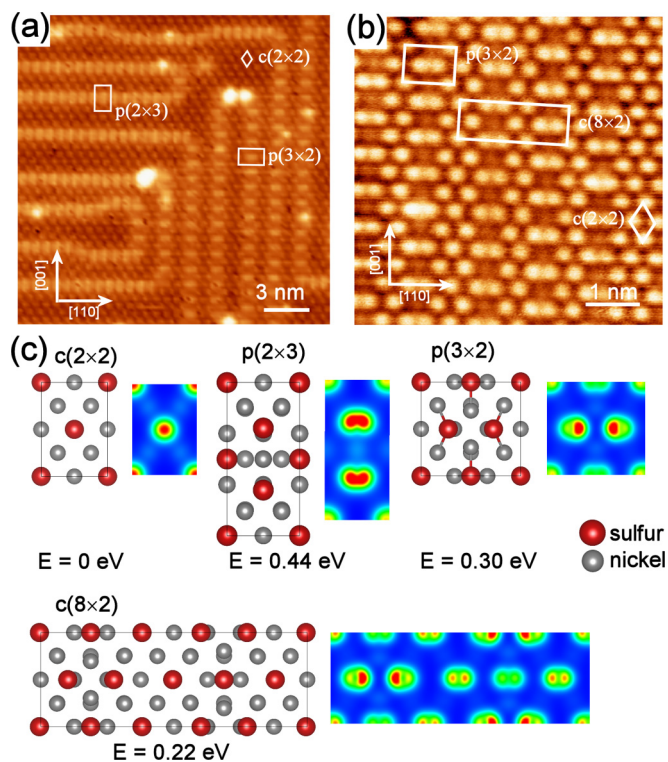

FIG. 2. Sulfur superstructures formed on the Ni(110) surface after graphene growth. (a), (b) High-resolution STM images of sulfur-covered regions. Imaging parameters: (a) $V_s = +1.0$ V, $I = 0.1$ nA, (b) $V_s = +0.3$ V, $I = 0.1$ nA, $T = 78$ K. (c) Structural models of sulfur atoms adsorbed on the Ni(110) surface and the corresponding simulated STM images at $V_s = +0.3$ V. Adsorption energies are presented with respect to that of a single sulfur atom in the c(2 × 2) structure; the energy of c(2 × 2) was set to zero and other values are given relative to this; each energy is also denoted per sulfur atom.

direct interaction between the substrates and graphene. However, we did not observe clear moiré patterns in the internal region of the SLG islands, which suggests that the SLG did not directly contact the substrate. Such a decoupling probably occurs upon cooling to room temperature, owing to the difference in the thermal expansion coefficients of Ni and graphene [50–54]. It is also possible that the remaining carbon atoms that did not contribute to the growth of graphene and instead formed a structurally disordered phase, such as a dilute phase of carbon (e.g., nickel carbide) [26,55,56], at the interface between SLG and Ni(110). This disordered phase could act as a decoupler for SLG islands from the substrate.

Closer inspection of the sulfur-covered region revealed that the line features are formed by sulfur atoms rearranged in local p(2 × 3) and p(3 × 2) periodicities in the c(2 × 2)-S phase [Fig. 2(a)]. The precise atomic configurations of sulfur in these structures are suggested by comparison between experimental and simulated STM images [Figs. 2(b) and 2(c)]. Both the p(2 × 3)-S and p(3 × 2)-S structures accommodate surplus sulfur atoms positioned in adjacent hollow sites and bridge sites within their unit cells [Fig. 2(c)]. Such a rearrangement of the sulfur atoms in two adjacent hollow sites of the nickel surface changes the orientation of the $3p$ orbitals of the sulfur atom to point toward the vacuum, whereas the corresponding orbitals originally lie in plane in the c(2 × 2)-S structure. This rearrangement of the electronic structure of the sulfur atoms resulted in an enhancement of the contrast in the STM image at higher sample biases. Consequently, the rows of the p(2 × 3)-S and p(3 × 2)-S are observed as horizontal and vertical lines in the c(2 × 2)-S phase, as shown in Figs. 1(c) and 2(a). Furthermore, these line features are separated by various widths of the c(2 × 2)-S structure, which prevent the line features from adjoining each other.

The coverage (Θ) by sulfur atoms in both the p(2 × 3) and p(3 × 2) phases was 0.67, whereas it was 0.5 for c(2 × 2). Quantitatively, our DFT computation showed that the p(2 × 3)-S and p(3 × 2)-S phases are approximately 0.44 eV and 0.30 eV per sulfur atom less stable than the c(2 × 2)-S phase. Thus, these structures are locally stressed at the surface. Another compressed structure, which was found less often than the others, was c(8 × 2)-S [$\Theta = 0.625$, approximately 0.22 eV per sulfur atom less stable than c(2 × 2)-S], as seen in Fig. 2(b). This structure also includes a pair of sulfur atoms arranged in the adjacent hollow sites, but their coverage is not as high as those of the p(2 × 3)-S and p(3 × 2)-S phases due to the larger unit cell. The p(3 × 2) and c(8 × 2) structures associated with sulfur atoms were previously observed by introducing an excess dose of sulfur from H_2S onto clean Ni(110) surfaces [44,45]. Although the nickel substrate used in this study contained an amount of sulfur impurity equivalent to 300 layers of the c(2 × 2)-S structure, we did not observe these compressed sulfur structures in the absence of the growth of graphene islands. This was confirmed by STM and LEED observations of a pristine Ni(110) crystal without carbon doping, which showed the presence of only the c(2 × 2)-S surface (Fig. S5 in the Supplemental Material [42]), even after it had been subjected to a similar heating process to that of the carbon-doped sample shown in Fig. 1.

Furthermore, AES elemental mapping revealed that no sulfur signal was detected from the SLG islands (Fig. S1 in the Supplemental Material [42]), indicating that the graphene neither grows over the sulfur atoms adsorbed on the substrate nor is adsorbed by sulfur atoms (an example of a minor exception can be found in Fig. S4 in the Supplemental Material [42]). In other words, the SLG islands and the sulfur superstructures are phase separated in general. These facts are also reasonably explained by the DFT calculations; compared with a single sulfur atom adsorbed on a clean nickel surface, a single sulfur atom placed on SLG is less stable by 3.80 eV, one placed at the interface between the nickel and SLG is less stable by 3.65 eV, and one placed in c(2 × 2)-S at the interface between the nickel and SLG is less stable by 0.75 eV (Fig. S6). From these observations, we conclude that the vertical and horizontal line features associated with the local sulfur atom rearrangements are created as a result of the compression of the c(2 × 2)-S phase derived from the expansion of the graphene island.

B. Real-time observation of graphene growth on the Ni(110) surface

Real-time observation of the growth of a graphene island by means of PEEM provided valuable clues as to the mechanism of growth of graphene on the Ni(110) surface. Figure 3(a) shows a snapshot image of graphene islands from a collection of PEEM images recorded over 2000 s (see supplemental video). Here, we focus on the graphene islands labeled island 1 and island 2; both of these islands had almost rectangular shapes. The reason why island 1 had a strong anisotropy between the [$\bar{1}$10] and [001] orientations is unclear from these observations. The dark regions observed on island 1 correspond to an adlayer of graphene. To investigate the growth rate of the graphene islands, cross-sectional signals along the lines AA', BB', and CC', as shown in Fig. 3(a), were collected from the PEEM images at various times and are plotted in Fig. 3(b). The rearranged data as a function of time indisputably show that all the island-edge positions changed linearly with time in both the [$\bar{1}$10] and [001] orientations during the initial stage of graphene growth. For instance, edge 1 in Fig. 3(b) moved at a constant speed of 38 nm/s toward the [$\bar{1}$10] orientation throughout the observation, whereas edge 2 moves at a speed of 31 nm/s, similar to that of edge 1, toward the [110] orientation for up to 1300 s and then slowed down due to its proximity to the neighboring graphene island. Similarly, other edges experienced linear growth rates in the early stages of growth, followed by deviation from the initial growth rate after certain elapsed times.

The linear growth rate with respect to time is evidence for progress of the growth of the graphene island by attachment of carbon atoms to the island edges. This is consistent with a recent report on observations of graphene growth on a Ni(111) surface by high-speed STM [57]. It also indicates that the carbon atoms were supplied exclusively at the edges of islands from the subsurface [path III in Fig. 3(c)]. If the carbon atoms were supplied by surface segregation to the interface between a graphene island and the substrate followed by diffusion to the growth front [path I in Fig. 3(c)] or by segregation to the c(2 × 2)-S regions far from the island followed by surface diffusion to the growth front [path II in Fig. 3(c)], the growth rate would have shown deviation from a linear trend.
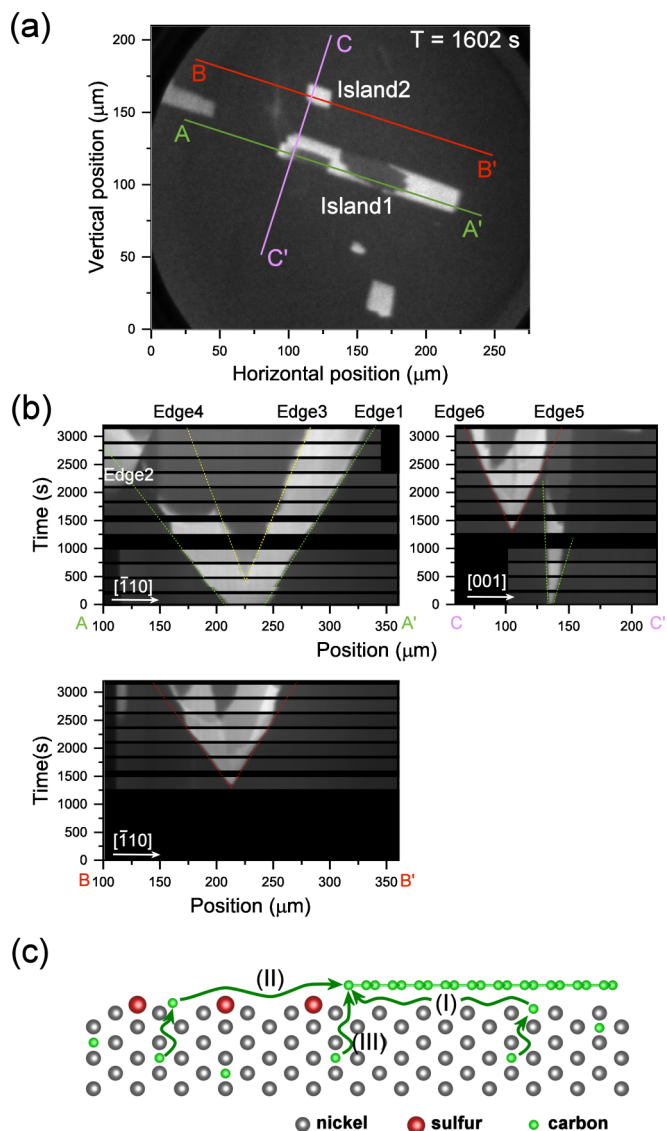
FIG. 3. Evolution of graphene size with time. (a) A snapshot image from a PEEM study of graphene growth at 1602 s after the sample temperature was set to 730 °C. (b) Size evolution of a graphene island with time. PEEM images sliced at the lines AA', BB' and CC' represented in (a) are arranged by time, revealing that the size of the graphene island increases almost linearly with time during the early stages of growth. (c) Possible paths for carbon atoms to attach to the edge of a graphene island: segregation and surface diffusion from inside (I) or outside (II) the graphene island or segregation to attach directly to the graphene island edge (III).

C. Mechanism of strong suppression of graphene growth on the Ni(110)-c(2 × 2)-S surface

To determine the mechanism by which a sulfur-covered nickel surface inhibits graphene growth, we calculated the relative energy of formation of a carbon atom placed at various depths in 12-layer Ni slabs with clean and c(2 × 2)-S surfaces (Fig. 4). For a clean Ni(110) surface, a carbon atom is most stable when it is located in the first layer and on the surface. This result is as expected from the tendency of multilayer graphene to form on a clean nickel surface. In contrast, the
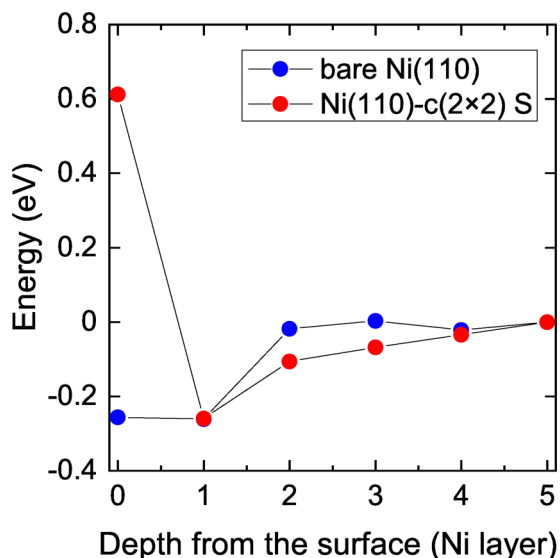

FIG. 4. Relative stability of a carbon atom residing at various depths from the surface of a 12-layer nickel slab. The energies of a carbon atom placed at various depths from the surface calculated by using a 12-layer Ni(110) slab model with a clean surface (blue dot) or with the c(2 × 2)-S surface (red dot). The energy is set to zero for a carbon atom placed in the fifth layer.

energy of a carbon atom increases markedly when it is placed on a c(2 × 2)-S surface. Because of this large instability, carbon atoms diffusing from the bulk to the surface are subjected to large repulsive forces by a topmost sulfur layer. This effect would prevent carbon atoms in the bulk from segregating to the sulfur-covered regions. Furthermore, a carbon atom placed between SLG and a nickel substrate is 2.25 eV less stable than one placed on a clean nickel surface (Fig. S6). This suggests that the segregation of carbon atoms is also unlikely to occur under graphene. These theoretical observations are consistent with the above suggestion made that segregation of the carbon atoms takes place only near the edges of graphene islands, as found in our PEEM observations (Fig. 3).

We were surprised to observe that sulfur atoms adsorbed on a nickel surface were an obstacle to the growth of graphene because it can generally grow over defects and steps. The difference in our growth process arises because repulsion between carbon and sulfur exists even in the topmost surface. Our DFT calculation showed that a sulfur atom placed near a graphene edge on a nickel slab is forcibly displaced from the region near the edge (Fig. S7). Moreover, the energy barrier for the diffusion of a sulfur atom in the c(2 × 2)-S phase was estimated to be 1.13 eV (Fig. S8), which is quite small compared with the energy reduction produced by graphene growth through segregation of carbon atoms (∼3.06 eV; see the section "Estimation of the energy reduction by graphene growth" in the Supplemental Material). After its nucleation, therefore, a small graphene island expands in area through the supply of carbon atoms to its edges from the bulk and by pushing aside sulfur atoms, as shown in Figs. 5(a)–5(d).

Once the precise arrangement of sulfur atoms adsorbed on the nickel surface was determined by STM and DFT, the formation of the line features observed in Figs. 1(c) and
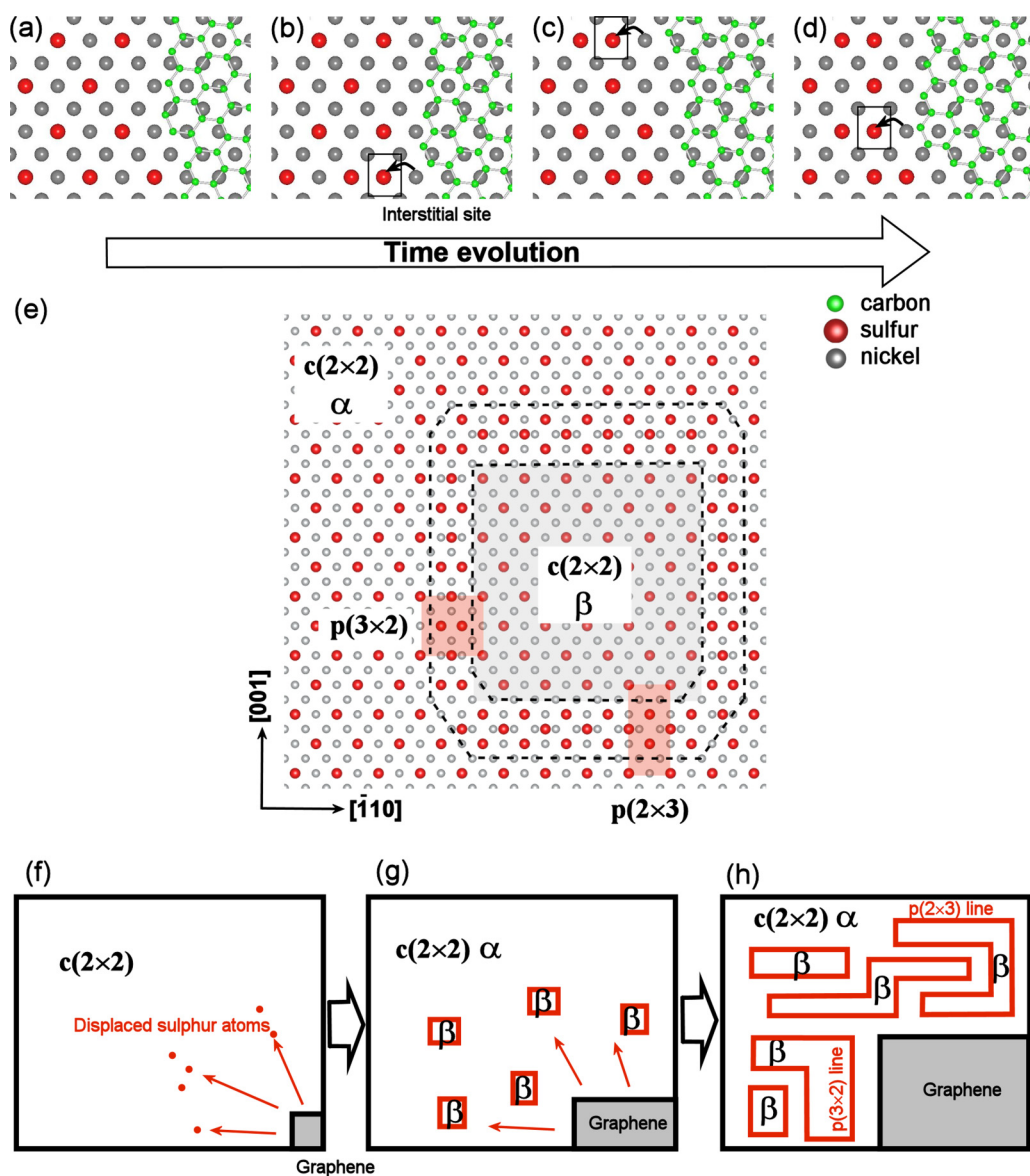
FIG. 5. Model for the formation of sulfur line features. (a)–(d) As carbon atoms become attached to the graphene edge, sulfur atoms are displaced to an interstitial site of c(2 × 2). (e) Two domains of c(2 × 2)-S (α and β) separated by a closed loop consisting of p(2 × 3)-S and p(3 × 2)-S lines. (f)–(h) Evolution of line features in a c(2 × 2)-S region made of excess sulfur atoms displaced as a result of graphene growth.

2(a) could be explained by means of a simple model for the creation of new c(2 × 2)-S domains. Because the domain of the c(2 × 2) periodicity is shifted by the lattice constant of Ni(110) across the p(2 × 3) or p(3 × 2) lines, these lines should form a closed loop separating the original domain of the c(2 × 2)-S (α-domain) from the new domain (β-domain) [Fig. 5(e)]. As the graphene grows, displaced sulfur atoms diffuse through the interstitial sites in the c(2 × 2) region [Fig. 5(f)], and p(2 × 3)-S and p(3 × 2)-S unit cells are created locally. Our DFT calculations demonstrated that these structures preferentially form one-dimensional lines that have lower energies by 0.2–0.4 eV per unit cell, compared with those produced by kinking or which exist individually (Fig. S9 in the Supplemental Material [42]). Accordingly, as the density of these structures increases, they form lines of a closed loop and a new β-domain is produced [Fig. 5(g)]. A further supply of sulfur as a result of graphene growth

creates complex one-dimensional patterns [Fig. 5(h)]. Interestingly, placing two one-dimensional line structures next to one another causes an instability of more than 0.1 eV per unit cell (Fig. S10 in the Supplemental Material [42]). Thus, two lines remain some distance apart owing to the repulsive forces, which also plays a role in the formation of the intricate patterns.

IV. CONCLUSIONS

We have obtained comprehensive experimental and theoretical evidence for the strong suppression of the growth of graphene layers in the presence of sulfur atoms on a Ni(110) surface. The rate of growth of graphene is markedly reduced on a Ni(110) surface covered with the c(2 × 2)-sulfur superstructure. The major effect that hinders graphene growth is repulsion between carbon and sulfur atoms on the nickel

surface. The topmost sulfur layer restrains segregation of carbon atoms from the bulk, and even inhibits lateral expansion of graphene islands; these two effects produce an extreme retardation of the growth process despite the presence of a rich carbon source in the nickel substrate. Optimization of the concentration of sulfur atoms at the surface by using an external sulfur source should permit finer control of the growth rate of graphene, the size of graphene islands, and the number of layers. Furthermore, patterning of sulfur-adsorbed areas by techniques such as mask deposition or lithography might be used as a template to produce desired shapes and sizes of SLG or graphene a few layers thick, including graphene nanoribbons.

[1] S. V. Morozov, K. S. Novoselov, M. I. Katsnelson, F. Schedin, D. C. Elias, J. A. Jaszczak, and A. K. Geim, Giant Intrinsic Carrier Mobilities in Graphene and its Bilayer, Phys. Rev. Lett. **100**, 016602 (2008).

[2] A. H. Castro Neto, F. Guinea, N. M. R. Peres, K. S. Novoselov, and A. K. Geim, The electronic properties of graphene, Rev. Mod. Phys. **81**, 109 (2009).

[3] A. A. Balandin, S. Ghosh, W. Bao, I. Calizo, D. Teweldebrhan, F. Miao, and D. N. Lau, Superior thermal conductivity of single-layer graphene, Nano Lett. **8**, 902 (2008).

[4] F. Liu, P. Ming, and L. Li, Ab initio calculation of ideal strength and phonon instability of graphene under tension, Phys. Rev. B **76**, 064120 (2007).

[5] F. Scarpa, S. Adhikari, and A. S. Phani, Effective elastic mechanical properties of single layer graphene sheets, Nanotechnology **20**, 065709 (2009).

[6] R. J. Young, I. A. Kinloch, L. Gong, and K. S. Novoselov, The mechanics of graphene nanocomposites: A review, Compos. Sci. Technol. **72**, 1459 (2012).

[7] C. Lee, J. Y. Kim, S. Bae, K. S. Kim, B. H. Hong, and E. J. Choi, Optical response of large scale single layer graphene, Appl. Phys. Lett. **98**, 071905 (2011).

[8] H. A. Hafez, S. Kovalev, J.-C. Deinert, Z. Mics, B. Green, N. Awari, M. Chen, S. Germanskiy, U. Lehnert, J. Teichert, Z. Wang, K.-J. Tielrooij, Z. Liu, Z. Chen, A. Narita, K. Müllen, M. Bonn, M. Gensch, and D. Turchinovich, Extremely efficient terahertz high-harmonic generation in graphene by hot Dirac fermions, Nature (London) **561**, 507 (2018).

[9] O. V. Yazyev, Emergence of magnetism in graphene materials and nanostructures, Rep. Prog. Phys. **73**, 056501 (2010).

[10] W. Han, R. K. Kawakami, M. Gmitra, and J. Fabian, Graphene spintronics, Nat. Nanotechnol. **9**, 794 (2014).

[11] Y. W. Son, M. L. Cohen, and S. G. Louie, Half-metallic graphene nanoribbons, Nature (London) **444**, 347 (2006).

[12] X. Li, W. Cai, J. An, S. Kim, J. Nah, D. Yang, R. Piner, A. Velamakanni, I. Jung, E. Tutuc, S. K. Banerjee, L. Colombo, and R. S. Ruoff, Large-area synthesis of high-quality and uniform graphene films on copper foils, Science **324**, 1312 (2009).

[13] M. R. Habib, T. Liang, X. Yu, X. Pi, Y. Liu, and M. Xu, A review of theoretical study of graphene chemical vapor deposition synthesis on metals: Nucleation, growth, and the role of hydrogen and oxygen, Rep. Prog. Phys. **81**, 036501 (2018).

[14] X. Li, W. Cai, L. Colombo, and R. S. Ruoff, Evolution of graphene growth on Ni and Cu by carbon isotope labeling, Nano Lett. **9**, 4268 (2009).

[15] R. S. Weatherup, A. J. Shahani, Z. J. Wang, K. Mingard, A. J. Pollard, M. G. Willinger, R. Schloegl, P. W. Voorhees, and S. Hofmann, In situ graphene growth dynamics on polycrystalline catalyst foils, Nano Lett. **16**, 6196 (2016).

[16] M. Eizenberg and J. M. Blakely, Carbon monolayer phase condensation on Ni(111), Surf. Sci. **82**, 228 (1979).

[17] M. Eizenberg and J. M. Blakely, Carbon interaction with nickel surfaces: Monolayer formation and structural stability, J. Chem. Phys. **71**, 3467 (1979).

[18] K. S. Kim, Y. Zhao, H. Jang, S. Y. Lee, J. M. Kim, K. S. Kim, J.-H. Ahn, P. Kim, J.-Y. Choi, and B. H. Hong, Large-scale pattern growth of graphene films for stretchable transparent electrodes, Nature (London) **457**, 706 (2009).

[19] A. Reina, X. Jia, J. Ho, D. Nezich, H. Son, V. Bulovic, M. S. Dresselhaus, and J. Kong, Large Area, Few-layer graphene films on arbitrary substrates by chemical vapor deposition, Nano Lett. **9**, 30 (2009).

[20] Q. K. Yu, J. Lian, S. Siriponglert, H. Li, Y. P. Chen, and S.-S. Pei, Graphene segregated on Ni surfaces and transferred to insulators, Appl. Phys. Lett. **93**, 113103 (2008).

[21] L. Baraton, Z. B. He, C. S. Lee, C. S. Cojocaru, M. Chatelet, J.-L. Maurice, Y. H. Lee, and D. Pribat, On the mechanisms of precipitation of graphene on nickel thin films, Europhys. Lett. **96**, 46003 (2011).

[22] H. Cao, Q. Yu, R. Colby, D. Pandey, C. S. Park, J. Lian, D. Zemlyanov, I. Childres, V. Drachev, E. A. Stach, M. Hussain, H. Li, S. S. Pei, and Y. P. Chen, Large-scale graphitic thin films synthesized on Ni and transferred to insulators: structural and electronic properties, J. Appl. Phys. **107**, 044310 (2010).

[23] R. S. Weatherup, B. Dlubak, and S. Hofmann, Kinetic control of catalytic CVD for high-quality graphene at low temperatures, ACS Nano **6**, 9996 (2012).

[24] A. Cabrero-Vilatela, R. S. Weatherup, P. Braeuninger-Weimer, S. Caneva, and S. Hofmann, Towards a general growth model for graphene CVD on transition metal catalysts, Nanoscale **8**, 2149 (2016).

[25] B. Dai. L. Fu, Z. Zou, M. Wang, H. Xu, S. Wang, and Z. Liu, Rational design of a binary metal alloy for chemical

vapour deposition growth of uniform single-layer graphene, Nat. Commun. **2**, 522 (2011).

[26] J. Lahiri, T. S. Miller, A. J. Ross, L. Adamska, I. I. Oleynik, and M. Batzill, Graphene growth and stability at nickel surfaces, New J. Phys. **13**, 025001 (2011).

[27] M. Xu, D. Fujita, K. Sagisaka, E. Watanabe, and N. Hanagata, Production of extended single-layer graphene, ACS Nano **5**, 1522 (2011).

[28] R. S. Weatherup, C. Baehtz, B. Dlubak, B. C. Bayer, P. R. Kidambi, R. Blume, R. Schloegl, and S. Hofmann, Introducing carbon diffusion barriers for uniform, high-quality graphene growth from solid sources, Nano Lett. **13**, 4624 (2013).

[29] H. Guo, J. Gao, N. Ishida, K. Sagisaka, and D. Fujita, Growth of quadrilateral graphene flakes with a sulfur atomic template on the surface of Ni (110), Carbon **153**, 116 (2019).

[30] J.-J. Lander, H. E. Kern, and A. L. Beach, Solubility and diffusion coefficient of carbon in nickel: Reaction rates of nickel-carbon alloys with barium oxide, J. Appl. Phys. **23**, 1305 (1952).

[31] K. Natesan and T. F. Kassner, Thermodynamics of carbon in nickel, iron-nickel and iron-chromium-nickel alloys, Metall. Trans. **4**, 2557 (1973).

[32] H. Guo, J. Gao, N. Ishida, M. Xu, and D. Fujita, Characterization of two-dimensional hexagonal boron nitride using scanning electron and scanning helium ion microscopy, Appl. Phys. Lett. **104**, 031607 (2014).

[33] H. Guo, H. Itoh, C. Wang, H. Zhang, and D. Fujita, Focal depth measurement of scanning helium ion microscope, Appl. Phys. Lett. **105**, 023105 (2014).

[34] T. Yamasaki, A. Kuroda, T. Kato, J. Nara, J. Koga, T. Uda, K. Minami, and T. Ohno, Multi-axis decomposition of density functional program for strong scaling up to 82, 944 nodes on the K computer: Compactly folded 3D-FFT communicators in the 6D torus network, Comput. Phys. Commun. **244**, 264 (2019).

[35] W. Kohn and J. J. Sham, Self-consistent equations including exchange and correlation effects, Phys. Rev. **140**, A1133 (1965).

[36] P. E. Blöchl, Projector augmented-wave method, Phys. Rev. B **50**, 17953 (1994).

[37] J. Ihm, A. Zunger, and M. L. Cohen, Momentum-space formalism for the total energy of solids, J. Phys. C: Solid State Phys. **12**, 4409 (1979).

[38] J. P. Perdew, K. Burke, and M. Ernzerhof, Generalized Gradient Approximation Made Simple, Phys. Rev. Lett. **77**, 3865 (1996).

[39] S. Grimme, Semiempirical GGA-type density functional constructed with a long-range dispersion correction, J. Comput. Chem. **27**, 1787 (2006).

[40] G. Mills and H. Jónsson, Quantum and Thermal Effects in H2 Dissociative Adsorption: Evaluation of Free Energy Barriers in Multidimensional Quantum Systems, Phys. Rev. Lett. **72**, 1124 (1994).

[41] Y. Tateyama, T. Ogitsu, K. Kusakabe, and S. Tsuneyuki, Constant-pressure first-principles studies on the transition states of the graphite-diamond transformation, Phys. Rev. B **54**, 14994 (1996).

[42] See Supplemental Material at http://link.aps.org/supplemental/10.1103/PhysRevMaterials.6.034007 for additional experimental and computational data.

[43] D. R. Warburton, G. Thornton, D. Norman, C. H. Richardson, R. McGarth, and F. Sette, Determination of sulfur coordination to the two-fold hollow site of Ni(110) using polarisation-dependent SEXAFS, Surf. Sci. **189-190**, 495 (1987).

[44] F. Besenbacher, I. Stensgaard, L. Ruan, J. K. Nørskov, and J. K. Jacobsen, Chemisorption of H, O, and S on Ni(110): General trends, Surf. Sci. **272**, 334 (1992).

[45] L. Ruan, I. Stensgaard, E. Lægsgaard, and F. Besenbacher, A scanning tunneling microscopy investigation of the Ni(110)-p(4 × 1)s phase, Surf. Sci. **296**, 275 (1993).

[46] R. Bäcker and G. Hörz, Scanning tunneling microscopic investigations of the adsorption and segregation of carbon and sulfur on nickel single crystal surfaces, Fresenius' J. Anal. Chem. **353**, 757 (1995).

[47] J. Zhang, J. Wang, T. Niu, S. Wang, L. Zhenyu, and W. Chen, Elementary process for CVD graphene on Cu(110): Size-selective carbon clusters, Sci. Rep. **4**, 4431 (2015).

[48] Y. Murata, V. Petrova, B. B. Kappes, A. Ebnonnasir, I. Petrov, Y.-H. Xie, C. V. Ciobanu, and S. Kodambaka, Moiré superstructures of graphene on faceted nickel islands, ACS Nano **4**, 6509 (2010).

[49] A. V. Fedorov, A. Y. Varykhalov, A. Dobrotvorskii, A. G. Chikina, V. K. Adamchuk, and D. Y. Usachov, Structure of graphene on the Ni(110) surface, Phys. Solid State **53**, 1952 (2011).

[50] T. G. Kollie, Measurement of the thermal-expansion coefficient of nickel from 300 to 1000 K and determination of the power-law constants near the Curie temperature, Phys. Rev. B **16**, 4872 (1977).

[51] N. Mounet and N. Marzari, First-principles determination of the structural, vibrational and thermodynamic properties of diamond, graphite, and derivatives, Phys. Rev. B **71**, 205214 (2005).

[52] H. Ghasemi and A. Rajabpour, Thermal expansion coefficient of graphene using molecular dynamics simulation: A comparative study on potential functions, J. Phys.: Conf. Ser. **785**, 012006 (2017).

[53] A. N. Obraztsov, E. A. Obraztsova, A. V. Tyurnina, and A. A. Zolotukhin, Chemical vapor deposition of thin graphite films of nanometer thickness, Carbon **45**, 2017 (2007).

[54] S. J. Chae, F. Gunes, K. K. Kim, E. S. Kim, G. H. Han, S. M. Kim, H. J. Shin, S. M. Yoon, J. Y. Choi, M. H. Park, C. W. Yang, D. Pribat, and Y. H. Lee, Synthesis of large-area graphene layers on poly-nickel substrate by chemical vapor deposition: Wrinkle formation, Adv. Mater. **21**, 2328 (2009).

[55] A. Dahal and M. Batzill, Graphene-nickel interfaces: A review, Nanoscale **6**, 2548 (2014).

[56] F. C. Schouten, E. W. Kaleveld and G. A. Bootsma, AES-LEED-Ellipsometry study of the kinetics of the interaction of methane with Ni(110), Surf. Sci. **63**, 460 (1977).

[57] L. L. Patera, F. Bianchini, C. Africh, C. Dri. G. Soldano, M. M. Mariscal, M. Peressi, and G. Comelli, Real-time imaging of adatom-promoted graphene growth on nickel, Science **359**, 1243 (2018).

[58] K. Momma and F. Izumi, VESTA 3 for three-dimensional visualization of crystal, volumetric and morphology data, J. Appl. Crystallogr. **44**, 1272 (2011).